Thermal-hydraulic and thermo-mechanical simulations of Water-Heavy Liquid Metal interactions towards the DEMO WCLL Breeding Blanket design

P.A. Di Maio[a], P. Arena[b], F. D'Aleo[a], A. Del Nevo[b], M. Eboli[b], R. Forte[a], A. Pesetti[c]

[a]*Dipartimento di Energia, Ingegneria dell'Informazione e Modelli Matematici, Università di Palermo, Viale delle Scienze, 90128 Palermo, ITALY*
[b]*ENEA FSN-ING-PAN, C.R. Brasimone, 40032 Camugnano (BO), ITALY*
[c]*Department of Civil and Industrial Engineering, University of Pisa, 56122 Pisa, ITALY*

The Water-Cooled Lithium Lead breeding blanket concept foresees the eutectic lithium-lead (Pb-15.7Li) alloy being cooled by pressurized sub-cooled water (temperature 295-328 °C; pressure 15.5 MPa) flowing in double wall tubes. Therefore, the interaction between the Pb-15.7Li and water (e.g. tube rupture) represents one of the main safety concerns for the design and safety analysis. Available LIFUS5/Mod2 experimental data are employed to assess the performances of thermal-hydraulic and thermo-mechanic codes. Thermal-hydraulic simulations, by SIMMER-III code, are focused on the prediction of the thermodynamic interaction among the fluids. ABAQUS Finite Element code, used for the design activities, is adotped to perform the thermo-mechanic simulations, calculating the stress and strain fields of LIFUS5/Mod2 main vessel during the experiments. Code results are compared with the experimental data and the outcomes from the analyses are discussed, in order to derive conclusions on the code assessment.

Keywords: Breeding Blanket, water-liquid metal interactions, LIFUS5.

1. Introduction

The Water-Cooled Lithium Lead (WCLL) breeding blanket (BB) concept ([1]-[4]) adopts pressurized sub-cooled water as coolant and a Heavy Liquid Metal (HLM), namely Pb-15.7Li alloy, as neutron multiplier, tritium breeder and carrier. Cooling water flows inside the cooling circuit housed within the breeder and deputed to remove the heat power therein generated. Hence, as a consequence of a possible in-box LOCA occurring within the breeder zone, water-HLM interactions will take place and are considered pivotal for the WCLL BB design and safety analysis activities [5]. Research activities are ongoing to master phenomena and processes occurring during the postulated accident [6], [7], to enhance the predictive capability and reliability of numerical tools [8], [9], to validate the computer models and codes [10], as well as to qualify computer codes and procedures for their applications [8]-[10]. These activities are conducted using existing and new experimental programmes. Available LIFUS5 experiments are employed to assess the performances of thermal-hydraulic and thermo-mechanic codes.

Within this framework, ENEA C.R. Brasimone has adopted the LIFUS5 facility for the investigation of water-HLM interaction, carrying out experimental campaigns and starting validation activities of numerical codes [7], [10]-[12] in order to assess both the thermal-hydraulic and thermo-mechanical computer codes performances. At present LIFUS5/Mod2 data are the most reliable for this purpose and the only one where strain data during injection are recorded. Therefore, besides these tests neglect the chemical reaction between PbLi and water, which, in any case, is delayed in time with respect to the thermodynamic interaction, they are considered relevant for the preliminary validation of the codes. Indeed, the study is focussed on the thermodynamic interaction, which is the first phenomena occurring when the water is injected at higher pressure into a system of HLM at lower pressure (so-called Coolant Coolant Interaction, Ref. [5]).

2. LIFUS5/Mod2 facility description

LIFUS5/Mod2 (Refs. [11]-[14]) is designed to be operated with different HLMs, such as: Lithium-Lead and Lead-Bismuth eutectic alloys and pure Lead. The operation of the test facility has the objectives of 1) investigating relevant phenomena connected with the safety of HLM fast reactor designs and 2) developing and validating numerical models for simulation codes used in safety analysis. The facility consists of four main parts:

- vessel (S1), where HLM/water interactions occur with a volume of 100 liters;
- water tank (S2), pressurized by means of a gas cylinder connected on the top;
- dump tank (S3);
- liquid metal storage tank (S4).

More detail about volume of vessels, liquid metal and geometry can be found in [11].

The description of the THINS (Thermal-Hydraulic of Innovative Nuclear System) configuration of the facility is reported in Refs. [11]-[14] and it is shown in Fig. 1. The main vessel S1 is filled with HLM (Lead-Bismuth alloy) with a compressibility ratio of 30%. The test section is configured in order to have an axial-symmetric geometry. The configuration is set-up in order to reduce, as far as possible, perturbations due to structures inside the vessel. The water injection system enters from the bottom of S1 vessel in central position. The injector orifice is covered by a protective cap, which is broken by the pressure of the water jet at the beginning of the injection phase.

author's email: pietroalessandro.dimaio@unipa.it

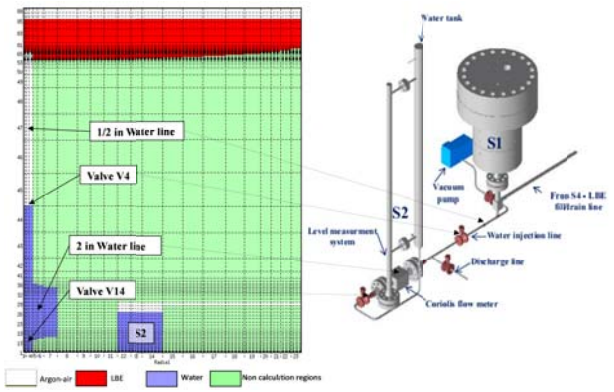

Fig. 1. LIFUS5/Mod2 facility and SIMMER-III geometrical model

The injection nozzle has an orifice of 4 mm diameter. The water line connects the tank S2 with the interaction vessel S1 towards valve V14, then the Coriolis flow meter and finally through valve V4. The water tank S2 is connected on the top with the gas line, which is used for setting and keeping the pressure of the water according with the test specifications.

The acquisition system acquires data at 1kHz and it is based on the following measurements:

- 73 thermocouples (TC): 68 installed on the test section inside the vessel; 2 on the vessel wall; 3 in the water tank and injection line for measuring the temperature of the injected water;
- 7 fast pressure transducers (PT): 4 measuring the pressure transient in the melt at different elevations and azimuthal angles; 1 installed on the top of the vessel S1; 1 on the bottom of the water tank (S2) and 1 the water injection line downstream the last valve;
- 6 high temperature strain gauges (SG) installed on the main vessel wall, for measuring the strain during the pressure transient. Five strain gauges are placed in a cross shape on the internal wall, whereas one is attached on the external wall in correspondence with the central internal SG, as shown in the following;
- 3 absolute pressure transducer (PC): 1 installed on the top flange of S1 (PC-S1V-01); 1 on the top of S2 and 1 in the gas line;
- 1 level measurement gauge mounted on the water tank support;
- 1 Coriolis flow meter placed on the water line.

3. Thermal-hydraulics

Thermal-hydraulic analyses [11] reproducing Test A2.4 [14] have been carried out by means of the SIMMER-III code [15], a numerical tool able to investigate effects of water-HLM interactions in terms of fluid-dynamic and thermal behaviour during postulated transient LOCA scenarios.

3.1 SIMMER-III model

The developed axisymmetric SIMMER-III geometrical domain of the LIFUS5/Mod2 facility is shown in the left side of Fig. 1, the main components of which are connected by dotted arrows to the real ones depicted in the overall sketch in the right of the same figure. The geometrical domain is composed by 23 radial and 88 axial mesh cells. Rotating the 2D SIMMER-III domain along the axis of symmetry the whole volumetric model is obtained, in which every cell is a toroidal volume with rectangular cross section.

The reaction vessel S1 was positioned in the upper part and coaxially to the model. The injection line is horizontally installed and cannot be coherently modelled in an axisymmetric domain. Therefore, to conserve the cylindrical shape of the injection tube, it was positioned vertically and coaxially with the entire model. This simplification entails almost 0.4 bar of gravity pressure losses in the SIMMER-III model.

The pressure time trends measured in the S2 dome is imposed as computational boundary condition of the performed simulation. The starting instant (t = 0 s) of the SIMMER-III calculation is assumed coincident with the instant when the water begins to flow through the injection valve. At the top of the injector, the injection orifice is kept closed for the lapse of time experimentally measured to achieve the cap rupture. The interruption of the water injection is simulated, as it occurs during the whole campaign, by the valve V4 closure, which isolates the vessel S1 from the pressurized water tank S2.

3.2 Numerical results

Test A2.4 starts with S1 filled with HLM at 1 bar and 400°C and the water tank and injection line set at 16 bar and 200 C (sub-cooling 1°C). The experimental pressure time trends of the test are shown in Fig. 2.

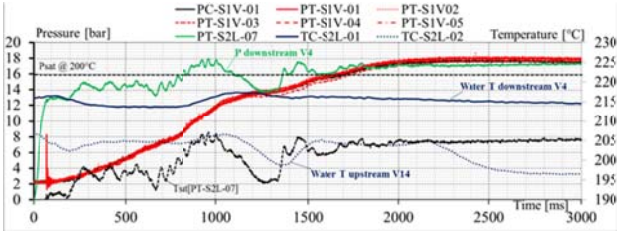

Fig. 2. Test A2.4 - P and T data trends [0 – 3 s]

The calculated pressure (Fig. 3) in S2 is not reported, being imposed as in the experiment. Four phases are distinguished during the test: 1) pressurization of water injection line up to rupture cap occurrence [0 to 71 ms]; 2) pressure driven, two phase mixture water-HLM interaction up to pressures equalization in S1 and S2 [71 to 2000 ms]; 3) buoyancy driven, two-phase water-HLM interaction up to V4 injection valve closure [2000 to 2304 ms]; 4) gas phase water energy increase due to HLM temperature of 400°C [2304 ms to End of Test].

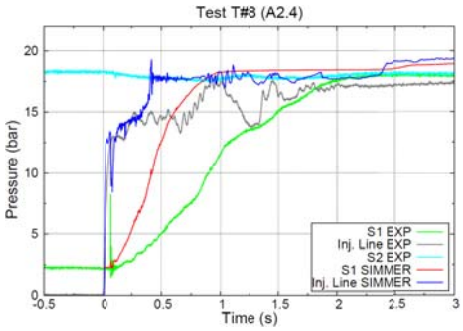

Fig. 3. Calculated and Experimental pressures of test A2.4

When the injection starts, SIMMER-III predicts a faster pressure increase in the injection line, up the cap rupture at 71 ms, being the pressure increase rate calculated by the code in the injection line 182.3 bar/s against 177.78 bar/s experimentally recorded. From this time on, a two phase mixture is injected in S1. The code slightly overestimates the experimental pressure upstream the injector up to 0.34 s. Then, the difference increases and the pressure calculated by the code rises faster up to the peak, occurring at 0.42 s and the equalization with the injection pressure (S2). In this phase, the pressure increase rate in the injection line calculated by the code is 12.37 bar/s against 5.76 bar/s of the experiment, while the pressure increase rate in S1 during phase 2 is 16.98 bar/s against 7.89 bar/s experimentally recorded by the pressure transducers. The different dynamic behaviour of the injection line can be explained by two main reasons: 1) the modelling of the injection line is simplified, because the piping in the Coriolis flow meter is neglected and roughly simulated adopting a Re independent energy loss coefficient, and the metallic structure are not modelled, thus neglecting friction losses; 2) the water in the injection line may have experienced local saturated conditions, because of the low margin from the saturation (1°C). Higher pressure and possible slightly lower temperature of the water upstream the injection are the main reasons why the calculated and experimental pressure trends in the interaction vessel S1 have different increase rates. This is demonstrated by the simulation of the Test A2.3 executed with the same boundary and initial conditions but with water at 180°C, thus having a sub-cooling equal to 21 C (Fig. 4).

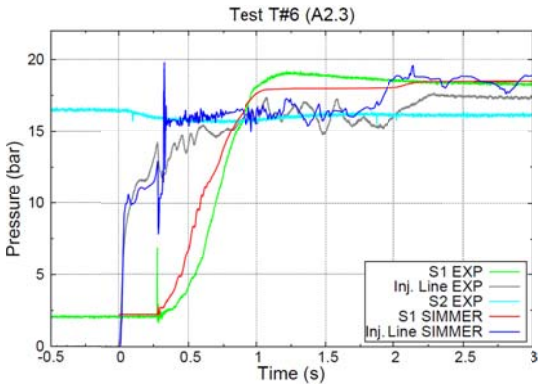

Fig. 4. Calculated and Experimental pressures of test A2.3

Due to this higher margin from saturation, the effect on the conditions of the water injected (i.e. void fraction) are reduced. Therefore, the uncertainties in predicting the pressure drop in the injection line and in the experimental set-up of the water temperature have a minor relevance. This implies that the pressure trends predicted by the code are more accurate and well represent the experimental data (see Fig. 4). Indeed, the pressure increase rate of the injection line calculated by the code is 46.2 bar/s up to injector break and 4.97 bar/s up to the pressure equalization, while the experimental trends are 51.2 bar/s and 3.1 bar/s, respectively. In S1 during phase 2, the pressure increase rates calculated by the code are 24.74 and 19.86 bar/s with an average of 22.36 bar/s. The experiment shows a pressure increase rate of 12.8 and 32.7 bar/s with an average of 22.37 bar/s. Finally, it must be mentioned that the modelling approach can improved using a two field thermal-hydraulic system code, e.g. RELAP5, for the water system (pipeline), and the SIMMER-III code for the zone where the interaction between the water and HLM occurs, thus where the application of a two fluids multi field code is unavoidable (Refs. [9],[16]).

4. Thermo-mechanical simulation

With the aim of qualifying a numerical procedure to be applied in order to reproduce and assess the effects of HLM-water interactions on the structure, the thermo-mechanical behaviour of the S1 vessel has been properly investigated setting up a Finite Element (FE) model of the aforementioned vessel and performing a pseudo-transient analysis.

4.1 FE model

A fully 3D FE model reproducing the S1 vessel and its pertinent attachment system has been set up, adopting a mesh composed of ~1.28 M nodes connected in ~1.16 M hexahedral linear elements. Both the complex system of bolts and the gasket have been properly reproduced (Fig. 5). In particular, special purpose solid elements, characterised by a membrane behaviour, have been adopted for the gasket. Concerning materials, a linear elastic behaviour has been considered for AISI 304, 316 and ASTM A193 B16, considering their thermo-mechanical properties depending only on temperature.

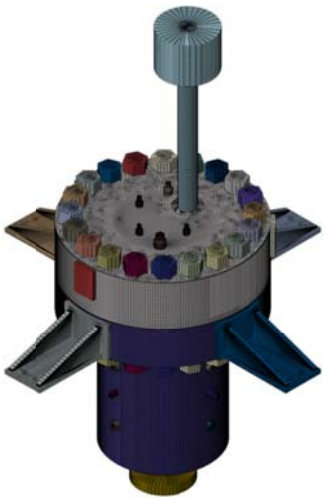

Fig. 5. The S1 vessel FE model

In order to reproduce the loading scenario relevant to the A2.4 experimental test, a consistent set of loads and boundary conditions has been imposed. From the thermal point of view, since the S1 vessel is insulated and no significant temperature ranges have been detected during water-HLM interactions, a uniform temperature field (400°C) has been considered. Concerning mechanical loads, a preload of 18.4 kN has been applied to the stud bolts connecting the top flange with the body, while the time-dependent pressure distribution measured by the PC-S1V-01 pressure transducer has been applied to all the internal surfaces of the reaction chamber. The gasket has been considered to be bonded with the body

of the vessel and in contact with the top flange. A friction model characterized by a uniform Coulombian friction factor equal to 0.25 has been adopted for the contact between the gasket and the top flange, as well as for that relevant to bolts and fasteners. All other components have supposed to be bonded.

The action of the attachment system has been properly reproduced by means of a set of mechanical restraints applied to S1 vessel sustaining shelves. In particular, in order to accommodate thermal strains, it has been allowed the radial expansion of the system.

4.2 Pseudo-transient analysis

A sequence of static mechanical analyses has been run in order to reproduce the whole duration of the A2.4 experimental test, neglecting the system inertia (no damping and no acceleration of the structure) and implementing the time-dependent pressure distribution experimentally measured by PC-S1V-01 and sampled with a frequency of 1 Hz. In particular, in order to validate the set up numerical model, results carried out in terms of strains have been benchmarked against experimental ones, obtained from the 6 strain gauges allocated onto both the internal and external surfaces of S1 vessel along the circumferential direction. The position of each SG has been identified in the FE model as shown in Fig. 6. SG-06 is located on the outer surface of the vessel at the same quote of the SG-04.

In order to support the validation of the FE model, its numerical predictions have been compared also with those of a theoretical-analytical model purposely set-up assuming the vessel to be a homogeneous, isotropic, axial-symmetric and linear elastic domain that undergoes pressure loads on its inner and outer surfaces. According to the continuum mechanics theory, the circumferential strain radial distribution on a cylindrical pressure vessel under plain strain condition is described by the following equation [17]:

$$\varepsilon_\phi(r)=\frac{1}{E}\left[(1+\nu)(p_i-p_e)\frac{R_e^{\,2}}{R_e^{\,2}-R_i^{\,2}}\frac{R_i^{\,2}}{r^2}+\frac{(1-2\nu)}{R_e^{\,2}-R_i^{\,2}}\left(p_iR_i^{\,2}-p_eR_e^{\,2}\right)\right]+\alpha\theta \quad (1)$$

where ε_ϕ is the circumferential strain, E is the Young modulus, ν is the Poisson coefficient, p_i and p_e are internal and external pressures, R_i and R_e are internal and external radii, α is the isotropic thermal expansion coefficient and θ is the relative thermal field.

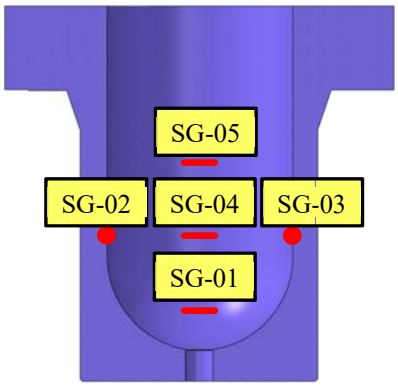

Fig. 6. Strain Gauge position

Numerical results obtained show a fairly good agreement with the pertaining experimental data measured by strain gauges located on the internal surface. In particular, the best matching is obtained in correspondence of the position of SG-01 and SG-02, where numerical predictions slightly deviate from experimental data up to a maximum error of 2%. Differently, concerning SG-03, SG-04 and SG-05, errors ranging between 6% and 10% are obtained. As far as the outer surface is concerned, the numerical results obtained in correspondence of SG-06 position show significant errors. On the other hand, the comparison between analytical and numerical predictions shows a really good match both on the inner and the outer surfaces of the vessel, suggesting, hence, the possibility of an imperfect functioning of SG-06.

Results obtained by FE simulation have been then benchmarked against both experimental and theoretical data, computing the relative errors Δ among the three different models. In Fig. 7, errors computed between numerical results and experimental data, together with the pressure time-based distribution adopted, are shown. In particular, errors appear to be larger in the first seconds of the test to reach rather stabilized values going to its end. The higher errors observed at the beginning of the test can be justified by the presence of transient effect (i.e. pressure waves propagation) which have not been taken into account in the analysis.

For sake of brevity, only results computed at 25 s from the Start of Test have been reported in Tab. 1 and Fig. 8, where errors calculated among different models and the circumferential strain radial profile have been reported.

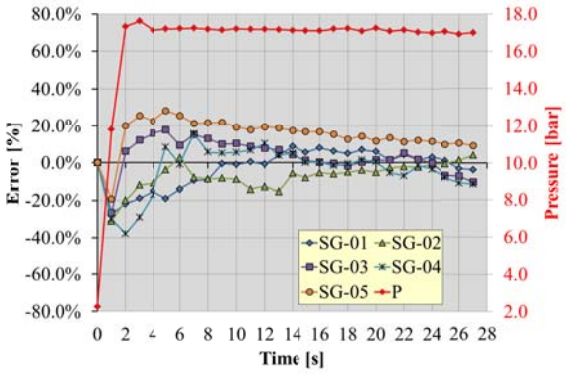

Fig. 7. Pressure applied and FEM-Exp errors

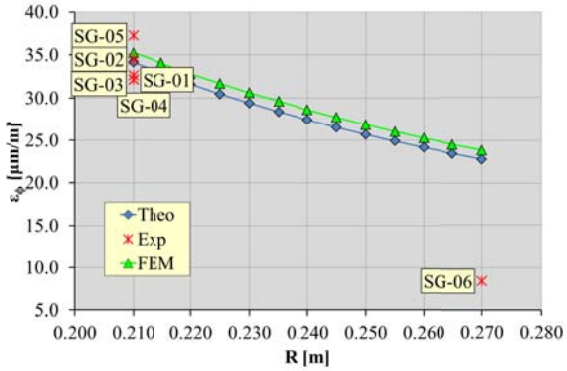

Fig. 8. Circumferential strain radial profile at End of Test

Tab. 1. Errors at End of Test

Strain	SG-01	SG-02	SG-03	SG-04	SG-05	SG-06
Theo [μm/m]	-34.18	-34.18	-34.18	-34.18	-34.18	-22.8
Exp [μm/m]	-32.18	-34.55	-32.69	-32.17	-37.27	-8.43
Δ [%]	-6.23	1.08	-4.55	-6.24	8.28	-170.42
FEM [μm/m]	-31.75	-34.66	-34.86	-34.65	-33.49	-24.2
Exp [μm/m]	-32.18	-34.55	-32.69	-32.17	-37.27	-8.43
Δ [%]	1.33	-0.31	-6.63	-7.69	10.13	-187.07
FEM [μm/m]	-31.75	-34.66	-34.86	-34.65	-33.49	-24.2
Theo [μm/m]	-34.18	-34.18	-34.18	-34.18	-34.18	-22.8
Δ [%]	7.11	-1.4	-1.99	-1.37	2.02	-6.16

5. Conclusions

With the aim of supporting the study of the "in-box-LOCA" and the associated phenomena for the WCLL BB, activities are conducted at ENEA C.R. Brasimone using both existing and new experimental campaigns in LIFUS5 facility. Available data relevant to HLM/water interactions, performed during THINS campaign, have been adopted to set up and to validate numerical codes towards the thermodynamic interaction occurring for the so-called Coolant Coolant Interaction. Indeed, this is representative of the first phenomena occurring during water leakage characterizing a LOCA scenarios in the WCLL breeding zone.

Thermal-hydraulic and thermo-mechanical analyses have been carried out using the LIFUS5/Mod2 Test A2.4. Pressure and temperature trends, as well as stress and strain distributions, have been calculated using the computer codes SIMMER and Abaqus. These results have been compared against the experimental data.

The thermal-hydraulic simulation has demonstrated that the pressure trend is correlated with the water mass injection. A reliable simulation of the two phase choked flow through the orifice, implies a good simulation of the pressure trend (i.e. Test A 2.3). On the opposite, minor differences in the void fraction at the break, larger in the simulation with respect to the experiment, cause the underestimation of the mass injected and therefore of the pressure gradient (i.e. Test A 2.4).

As to the thermo-mechanical simulation, a good match between experimental and numerical results has been achieved, with the except of the comparison between data collected by the external strain gauge (SG-06) and results calculated by Abaqus FEM code, probably due to an instrumentation malfunctioning. Moreover, non-negligible errors have been observed during the first phase of the experimental test, which could be justified by the reproduction of the transient by means of a sequence of static analyses, neglecting dynamic phenomena.

Acknowledgments

This work has been carried out within the framework of the EUROfusion Consortium and has received funding from the Euratom Research and Training Programme 2014–2018 under grant agreement no. 633053. The views and opinions expressed herein do not necessarily reflect those of the European Commission.

References

[1] A. Del Nevo, et al, WCLL breeding blanket design and integration for DEMO 2015: status and perspectives Fusion Eng. Des., 124 (2017), pp. 682-686.

[2] E. Martelli, et al, Advancements in DEMO WCLL breeding blanket design and integration, Int. J. of Energy Research, 42(1), 2018, pp. 27-52.

[3] A. Tassone, et al., Recent Progress in the WCLL Breeding Blanket Design for the DEMO Fusion Reactor, IEEE Transactions on Plasma Science, 46 (5), 2018, pp. 1446-1457.

[4] A. Del Nevo, et al., Recent progress in developing a feasible and integrated conceptual design of the WCLL BB in EUROfusion Project, Fusion Eng. Des.,(2019), https://doi.org/10.1016/j.fusengdes.2019.03.040.

[5] M. Eboli, et al, Simulation study of pressure trends in the case of loss of coolant accident in Water Cooled Lithium Lead blanket module, Fusion Eng. Des., 98–99 (2015), pp. 1763–1766

[6] M. Eboli, et al, Experimental activities for in-box LOCA of WCLL BB in LIFUS5/Mod3 facility, Fusion Eng. Des., (2019), https://doi.org/10.1016/j.fusengdes.2019.01.113.

[7] S. K. Moghanaki, et al, Validation of SIMMER-III code for in-box LOCA of WCLL BB: pre-test analysis of Test D1.1 in LIFUS5/Mod3 facility, Fusion Eng. Des., (2019), https://doi.org/10.1016/j.fusengdes.2019.01.131.

[8] M. Eboli, et al, Implementation of the chemical PbLi/water reaction in the SIMMER code, Fusion Eng. Des. 109-111 (2016) 468-473.

[9] B. Gonfiotti, et al, Development of a SIMMER/RELAP5 coupling tool, Fusion Eng. Des., (2019), https://doi.org/10.1016/j.fusengdes.2019.03.084.

[10] M. Eboli, et al, Post-test analyses of LIFUS5 Test#3 experiment, Fusion Eng. Des., 124 (2017), pp. 856-860.

[11] A. Pesetti, et al, Experimental investigation and SIMMER-III code modelling of LBE–water interaction in LIFUS5/Mod2 facility, Nuclear Engineering and Design, 290 (2015) 119-126

[12] A. Del Nevo, et al, Addressing the heavy liquid metal – Water interaction issue in LBE system, Progress in Nuclear Energy, 89 (2016) 204-212.

[13] P. Lorusso, et al, GEN-IV LFR development: Status & perspectives, Progress in Nuclear Energy, 105 (2018) 318-331.

[14] A. Del Nevo, et al, LIFUS5/Mod2 facility – Test A2.4 Experimental Data And Test Analysis Report, ENEA technical report L5-T-R-120, January 2015

[15] S. Kondo, et al, SIMMER III: a computer program for LMFR core disruptive accident analysis, O-arai

Engineering Centre, Japan Nuclear Cycle Development Institute, Research Document JNC TN 9400 2003-071
[16] A. Del Nevo, et. al, Experimental and Numerical Investigations of Interaction between Heavy Liquid Metal and Water for supporting the Safety of LFR Gen. IV Reactor Design, Proc. of the 16th Int. Topical Meeting on Nuclear Reactor Thermal Hydraulics (NURETH-16), Log Number: 13807 Hyatt Regency Chicago, Chicago, IL, USA, Aug. 30Sept. 4, 2015.
[17] J. Salençon, Handbook of Continuum Mechanics, Springer, August 2000, doi: 10.1007/978-3-642-56542-7